

Optical vector network analyzer for single-scan measurements of loss, group delay, and polarization mode dispersion

Dawn K. Gifford, Brian J. Soller, Matthew S. Wolfe, and Mark E. Froggatt

We present a method for measuring the complete linear response, including amplitude, phase, and polarization, of a fiber-optic component or assembly that requires only a single scan of a tunable laser source. The method employs polarization-diverse swept-wavelength interferometry to measure the matrix transfer function of a device under test. We outline the theory of operation to establish how the transfer function is obtained. We demonstrate the enhanced accuracy, precision, and dynamic range of the technique through measurements of several components. © 2005 Optical Society of America

OCIS codes: 120.4640, 120.3180, 120.5050.

In the context of high-speed, multiwavelength optical communication, it is becoming increasingly important to rigorously characterize individual components to ensure overall system performance. The Jones matrix (JM) or linear transfer function (TF) of a fiber-coupled component, when measured as a function of frequency, contains all of the information required to predict the final component performance (loss, dispersion, polarization dependence, etc.).¹ Spectral measurement of the TF of a device under test (DUT) requires stimulating multiple input polarization states at each wavelength, a process that can be complex and time consuming, typically requiring multiple measurement scans.² It has, however, been demonstrated that the TF of a component can be measured with a single measurement scan using a polarization-diverse interferometric technique.³

In this paper we describe a novel interferometric network for single-scan, high-resolution spectral measurements of the TF. In addition, we demonstrate mathematically how the TF is obtained from this measurement apparatus, an analysis not present in other works. We then show that highly accurate spectral amplitude and phase information can be extracted from the TF in the form of polarization-averaged group delay

(GD), polarization mode dispersion (PMD), and insertion loss (IL). Data are presented demonstrating, we believe for the first time, greater than 100, 80, and 60 dB dynamic ranges for the polarization-averaged IL, GD, and PMD measurements, respectively. The elimination of the need for multiple wavelength scans in combination with the accurate and sensitive nature of the interferometric measurement technique yields an instrument ideally suited for high-resolution metrology of passive optical components for high bit-rate network applications (e.g., tunable dispersion compensators, fiber Bragg gratings, arrayed waveguide gratings, etc.).

The measurement technique is based on swept-wavelength interferometry (SWI).³⁻⁵ The optical network used for our experiments is shown in Fig. 1. While similar in function to the network used in Ref. 2, this network architecture places the polarization conditioning interferometer “outside” the measurement interferometer and also eliminates a polarization beam combiner and the use of polarization-maintaining fiber and polarization-maintaining couplers.

In the network shown in Fig. 1, a tunable laser source (TLS) is used in combination with concatenated Mach-Zender interferometers, two polarization controllers, a polarization beam splitter, and three photodiodes labeled S, P, and A. The TLS used in these experiments was a Thorlabs Pico series tunable laser capable of mode-hop-free operation across the *C* and *L* communication bands with a specified linewidth of 200 kHz. The laser was tuned at 70 nm/s. Not shown are a wavelength reference

The authors are with Luna Technologies, 2020 Kraft Drive, Suite 2000, Blacksburg, Virginia 24060. D. K. Gifford's e-mail address is giffordd@lunatechnologies.com.

Received 21 March 2005; revised manuscript received 6 June 2005; accepted 30 June 2005.

0003-6935/05/347282-05\$15.00/0

© 2005 Optical Society of America

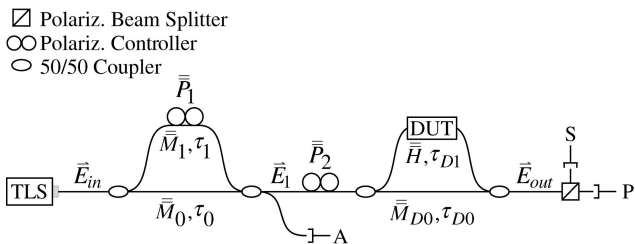


Fig. 1. Optical vector network analyzer.

(HCN gas cell) and an auxiliary interferometer. The NIST-calibrated wavelength reference is used to adjust for wavelength errors in the starting wavelength of a measurement scan. The auxiliary interferometer is used as a trigger to sample the incoming data in equal increments of optical frequency. This serves to correct for deviations from linearity in optical frequency during laser tuning and thus enable proper application of the Fourier transform processing described in following paragraphs.⁶ The use of both a gas cell and an auxiliary interferometer are well-known methods to correct for phase errors during laser tuning.

The interferometer closest to the TLS in Fig. 1 is used to create two time-shifted, orthogonal polarization states with which to simultaneously interrogate the DUT. We show that when this network is properly aligned, it can be used to measure the TF of the DUT in a single laser scan. For the purposes of this analysis, we assume a normalized input laser field of the form $\vec{E}_{in} = \hat{\rho} e^{-i\omega t}$, where $\hat{\rho}$ is a unit vector describing the state of polarization and ω is the instantaneous optical frequency. After passing through the first Mach-Zehnder interferometer, the field can be described by

$$\begin{aligned} \vec{E}_1 &= (\bar{M}_0 + \bar{M}_1) \hat{\rho} \exp(-i\omega t) \\ &= \hat{m} \exp[-i\omega(t - \tau_0)] + \hat{n} \exp[-i\omega(t - \tau_1)]. \end{aligned} \quad (1)$$

Here \bar{M}_0 and \bar{M}_1 are matrix operators that describe the propagation of the field through the two branches of the first interferometer, τ_0 and τ_1 are the delays associated with these branches, and \hat{m} and \hat{n} are two unit vectors describing the output states of polarization. The polarization controller, \bar{P}_1 , is used to modify the polarization state of the field in the upper branch of the interferometer such that \hat{m} and \hat{n} are orthogonal. In practice, this orthogonality condition can be established by minimizing the fringe amplitude at the detector labeled A in Fig. 1.

The second polarization controller, \bar{P}_2 , is then used to ensure that, after passing through the lower branch of the second interferometer, the field components associated with the two branches of the first interferometer are divided equally between the orthogonal polarization states defined by the polarization beam splitter, \hat{s} and \hat{p} .⁷ This condition is described by

$$\bar{M}_{D0} \bar{P}_2 \hat{m} = \frac{1}{\sqrt{2}} (\hat{s} + \hat{p}) \exp(i\omega\tau_{D0}), \quad (2)$$

$$\bar{M}_{D0} \bar{P}_2 \hat{n} = \frac{1}{\sqrt{2}} (\hat{s} - \hat{p}) \exp(i\omega\tau_{D0}), \quad (3)$$

where \bar{P}_2 is the TF of the second polarization controller, \bar{M}_{D0} is the matrix representing propagation through the lower branch of the second interferometer, and τ_{D0} is the delay associated with this branch. The field that propagates through the lower branch, termed the reference field, can then be written as

$$\begin{aligned} \vec{E}_{R,out} &= \bar{M}_{D0} \bar{P}_2 \vec{E}_1 \\ &= \frac{1}{\sqrt{2}} (\hat{s} + \hat{p}) \exp[-i\omega(t - \tau_0 - \tau_{D0})] \\ &\quad + \frac{1}{\sqrt{2}} (\hat{s} - \hat{p}) \exp[-i\omega(t - \tau_1 - \tau_{D0})]. \end{aligned} \quad (4)$$

The field that propagates through the upper branch of the second interferometer experiences a polarization-dependent loss and phase shift due to the DUT, which can be described by the DUT's TF, \bar{H} . This field can be expressed as

$$\begin{aligned} \vec{E}_{D,out} &= \bar{H} \bar{P}_2 \hat{m} \exp[-i\omega(t - \tau_0 - \tau_{D1})] \\ &\quad + \bar{H} \bar{P}_2 \hat{n} \exp[-i\omega(t - \tau_1 - \tau_{D1})], \end{aligned} \quad (5)$$

where τ_{D1} is the delay associated with the upper branch of the second interferometer.

The polarization beam splitter then splits the combined field, \vec{E}_{out} , into two orthogonal components \hat{s} and \hat{p} according to

$$\begin{aligned} E_s \hat{s} &= (\vec{E}_{out} \cdot \hat{s}) \hat{s} = \\ &\left(\frac{1}{\sqrt{2}} \{ \exp[-i\omega(t - \tau_0 - \tau_{D0})] + \exp[-i\omega(t - \tau_1 - \tau_{D0})] \} \right. \\ &\quad \left. + [(\bar{H} \bar{P}_2 \hat{m}) \cdot \hat{s}] \times \exp[-i\omega(t - \tau_0 - \tau_{D1})] \right. \\ &\quad \left. + [(\bar{H} \bar{P}_2 \hat{n}) \cdot \hat{s}] \times \exp[-i\omega(t - \tau_1 - \tau_{D1})] \right) \hat{s} \end{aligned} \quad (6)$$

$$\begin{aligned} E_p \hat{p} &= (\vec{E}_{out} \cdot \hat{p}) \hat{p} = \\ &\left(\frac{1}{\sqrt{2}} \{ \exp[-i\omega(t - \tau_0 - \tau_{D0})] - \exp[-i\omega(t - \tau_1 - \tau_{D0})] \} \right. \\ &\quad \left. + [(\bar{H} \bar{P}_2 \hat{m}) \cdot \hat{p}] \times \exp[-i\omega(t - \tau_0 - \tau_{D1})] \right. \\ &\quad \left. + [(\bar{H} \bar{P}_2 \hat{n}) \cdot \hat{p}] \times \exp[-i\omega(t - \tau_1 - \tau_{D1})] \right) \hat{p} \end{aligned} \quad (7)$$

It is important to note here that simple basis rotations applied to a TF have no effect on the linear parameters (GD, PMD, etc.) extracted from that TF.

We can apply a unitary and invertible rotation matrix, \bar{R} , and its inverse such that $\bar{H}\bar{P}_2 = \bar{H}\bar{P}_2\bar{R}^{-1}\bar{R}$. We then assume that the second polarization controller, \bar{P}_2 , is a simple rotation with negligible PMD such that $\bar{H}\bar{P}_2\bar{R}^{-1} = \bar{H}'$ is just a rotated version of the TF, \bar{H} . This constitutes the only major assumption of this analysis and limits the smallest measurable PMD value to the residual PMD in the controller, \bar{P}_2 , which is typically on the order of 5–10 fs.

We can then choose \bar{R} so that $\bar{R}\hat{m} = \hat{s}$ and $\bar{R}\hat{n} = \hat{p}$, a simple operation of rotating one set of orthogonal vectors into another. For simplicity, we now introduce a new notation such that $H_{sp} = (\bar{H}'\hat{s}) \cdot \hat{p}$. We also introduce two new variables, $\tau = \tau_1 - \tau_0$ and $\tau_D = \tau_{D1} - \tau_{D0}$. Using this notation and doing some algebra, one can show that the intensities at the two detectors, S and P, shown in Fig. 1, can be written as

$$I_p(\omega) = E_p E_p^* \propto \text{Re}\{H_{pp} \exp[i\omega(\tau_D + \tau)] - H_{sp} \exp[i\omega(\tau_D - \tau)]\} + \dots, \quad (8)$$

$$I_s(\omega) = E_s E_s^* \propto \text{Re}\{H_{ps} \exp[i\omega(\tau_D + \tau)] + H_{ss} \exp[i\omega(\tau_D - \tau)]\} + \dots. \quad (9)$$

In these equations, we have omitted several terms that do not relate directly to the extraction of the TF—specifically, terms with no delay, with delay τ , and with delay τ_D . The four terms, H_{pp} , H_{sp} , H_{ps} , and H_{ss} , in Eqs. (8) and (9) are the four elements of the DUT TF (including the fiber pigtailed and the polarization controller, \bar{P}_2) expressed in the orthogonal basis of the polarization beam splitter.

Examining Eqs. (8) and (9) one can see that as the TLS frequency is swept, fringes are generated as a function of time on the two detectors, S and P, at frequencies proportional to the delays $\tau_D + \tau$ and $\tau_D - \tau$. A discrete Fourier transform (FFT) of the data from each channel will reveal impulses at these delays. Three such impulses are shown in Fig. 2. This plot displays the FFT of raw data from the P detector. The DUT in this case was a fiber Bragg grating. The impulses at $\tau_D - \tau$ and $\tau_D + \tau$ are associated with two elements of the DUT TF.

The four impulses associated with the TF of the DUT (two from each detector) can be extracted by the process of bandpass filtering these four impulses and transforming them individually back to the optical frequency domain. This digital filtering process yields the four complex TF elements. The dashed-line boxes in Fig. 2 represent the location of windows used to extract the two impulses associated with the DUT TF in this data set. The windowing function used to process the data in this paper was a “Rect” function with the edges smoothed using a Gaussian curve to reduce ringing due to edge effects. While this choice of window works well, other functions can be used. The windowing function must be chosen such that it does not alter the DUT impulses and thus affect the mea-

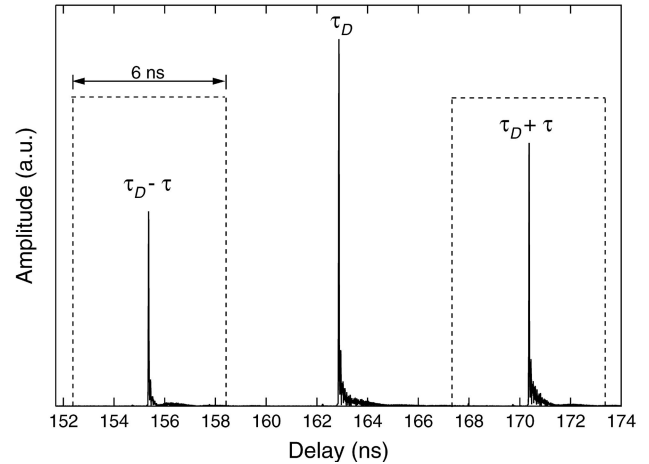


Fig. 2. FFT of raw data from detector P. The DUT is a fiber Bragg grating. The peaks at $\tau_D - \tau$ and $\tau_D + \tau$ are associated with two elements of the DUT TF. The dashed boxes represent the location of windows used to “slice out” these impulses to extract the DUT TF elements. The 6 ns width of these windows limits the measurable GD or PMD to 6 ns.

sured device response. Also, the window width must be wide enough to encompass all of the DUT impulse response, yet narrow enough not to include extraneous information from other peaks.

Any dispersiveness in the DUT causes the impulses associated with the TF elements to spread in time. This is well illustrated by the spreading of the Bragg grating impulses shown in Fig. 2. The delay difference, $\tau = \tau_1 - \tau_0$, must therefore be chosen such that the spreading does not cause the peaks to overlap in time. Such an overlap renders the TF elements “mixed” in the time domain and the process of filtering individual peaks becomes impossible. In this paper, a delay of about 6 ns was used. This value was chosen to give an effective wavelength resolution of ~ 1.5 pm. The chosen delay in turn limits the measurable GD and PMD ranges to 6 ns.

The delay difference in the interferometer used for triggered acquisition, τ_t , limits the delay of the DUT to no greater than $\tau_t/2$. The maximum τ_t is in turn limited by the scan speed of the laser and the sampling speed of the data-acquisition system used. For a current embodiment of the measurement system, DUT lengths are limited to <100 m in transmission and half that length in reflection.

Figure 3 shows the GD of an acetylene gas cell absorption line as measured using the technique described above. It is important to note here that a simple definition of GD as the derivative of the phase with respect to frequency yields a quantity that varies as a function of the input polarization state. When quantifying the GD of a component, then, it is preferable to calculate some average GD with respect to the polarization state. One common method to define an average is to find the GD associated with the principle states of polarization⁸ and average these two results.³ We find that this formulation yields a GD that becomes ill defined for components with high

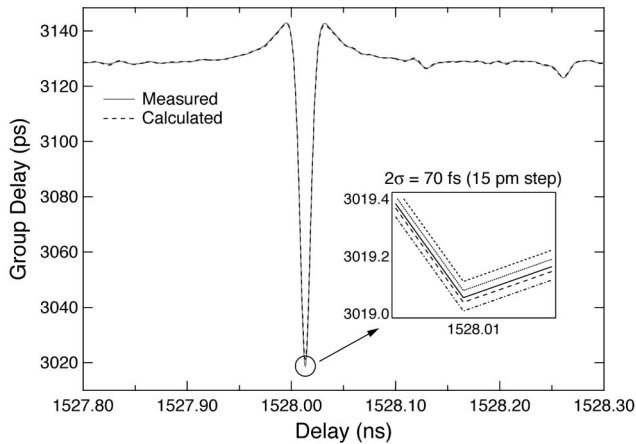


Fig. 3. Group delay of an acetylene gas cell as measured (solid curve) using the technique described in this paper and as calculated (dashed curve) from the loss of the same cell. The inset shows five representative data sets illustrating measurement repeatability.

polarization-dependent loss (PDL). Rather than use this definition, then, we calculate the GD from the measured TF using a slightly unconventional definition, a weighted average phase derivative:

$$GD(\omega) = \frac{\arg\{\sum H_{ij}(\omega)H_{ij}^*(\omega - \Delta\omega)\}}{\Delta\omega}, \quad (10)$$

where the sum is over the four matrix elements. This definition weights transmitting states more heavily than nontransmitting ones and thus yields more intuitive polarization-averaged results, even for components with nontransmitting states (e.g., a polarizer).

To demonstrate the precision of the GD measurement, 20 data sets with 32 scans averaged per set were recorded and compared. Each individual data set took less than 0.5 s to acquire. These data were taken using a 1.5 pm wavelength step. At the minimum of the absorption line, the 2σ variation of the GD is found to be 70 fs with a 15 pm derivative step size and 40 fs with a 30 pm step. These step sizes were chosen as they are most relevant to the metrology of components for narrowband, high bit-rate systems. The inset in Fig. 3 shows a representative subset of these data with a 15 pm step size. To check the accuracy of the GD measurement, we applied the Kramers–Kronig relationships to derive the GD from the measured loss through the gas cell.⁹ The calculated GD, shown as the dotted curve in Fig. 3, closely matches the measured GD. Note that the insertion loss of the gas cell was also measured with the technique described herein.

A measurement of the PMD of a calibrated artifact is shown in Fig. 4. The definition used in this paper to derive the PMD from the TF of a DUT is well established.⁸ While the PMD value quoted by the manufacturer of the artifact is 0.42 ps, we measure an average PMD across the wavelength range of the scan of 0.405 ps with a standard deviation of 0.01 ps.

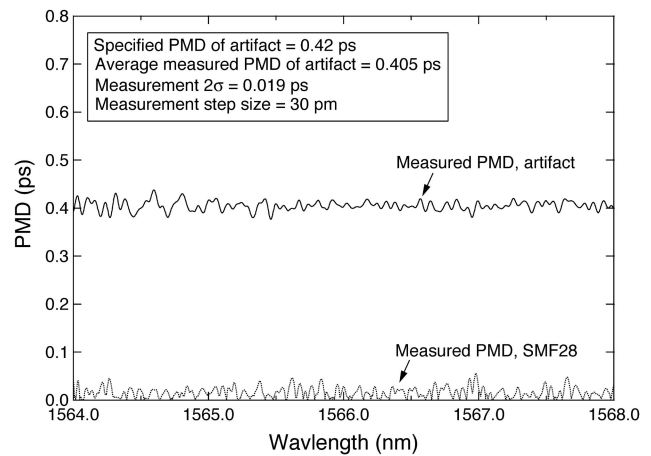


Fig. 4. Measured PMD of a PMD artifact (solid curve) and a 7 m length of SMF28 fiber (dotted curve) using the network shown in Fig. 1.

The small difference is well within the expected measurement error. To further verify the accuracy of the PMD measurement, we measured the PMD of a 7 m long SMF28 fiber. As is expected for this fiber, the measurement shows little PMD across the wavelength range of the scan (see Fig. 4). The standard deviation of this data set is again 0.01 ps. Both of these measurements were made using a 1.5 pm step and a 30 pm smoothing and derivative step. Each measurement took less than 1 min to acquire. For a step of 500 pm, the average measured PMD for the fiber is 8 fs, showing that the residual PMD of the measurement network is very small.

The coherent interferometric technique is ideal for metrology of narrowband dense wavelength division multiplexing (DWDM) components that may have wavelength-dependent loss features. To demonstrate this, we measured the TF of one channel of a fiber-coupled thin-film filter designed as a wavelength multiplexer. Figure 5 shows the GD and PMD derived from the measured TF of this filter. The maximum and minimum insertion loss (IL) as a function of wavelength, measured with the same technique and calculated from the TF, are also shown. The two IL curves shown in Fig. 5, IL_{\min} and IL_{\max} , were generated numerically using the TF and an eigenanalysis technique.¹⁰ For this component, the minimum and maximum are nearly identical across the passband of the device, indicating low PDL. One can see from Fig. 5 that the IL features are resolvable down to less than -100 dB. In addition, the GD and PMD are measurable at IL values down to -80 dB, demonstrating that this measurement technique enables dispersion characterization for components with very high loss.

The high dynamic range achieved in this paper is enabled first by the high sensitivity inherent in the homodyne interferometric technique, and second by careful averaging of multiple data sets. The averaging algorithm used first aligns the relative phases of each data set and then computes the mean by aver-

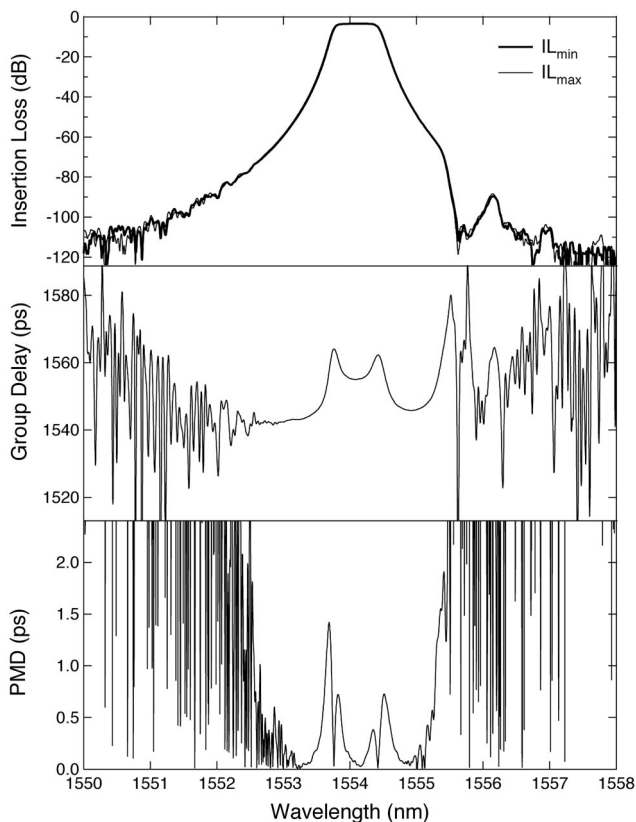


Fig. 5. Measured IL, GD, and PMD of a thin-film filter using the network shown in Fig. 1. The two IL curves represent the maximum and minimum IL as a function of input polarization state and wavelength.

aging real and imaginary parts. This ensures that small contributions from noise in both amplitude and phase average to zero. If, instead, the amplitude and phase are averaged, as is more common, noise contributions average to a small, but nonzero, number. This averaging method, then, allows improved access to the full sensitivity of the measurement technique, thereby enabling levels of dynamic range beyond 80 dB.

In this paper, we have concentrated on results for GD, PMD, and IL. Other quantities, such as chromatic dispersion, PDL, and second-order PMD, are easily calculated from the TF as well. Also, by use of a Fourier transform, one can easily examine the behavior of the DUT in the optical time domain, as is evident in Fig. 2. While we have concentrated on transmission devices in this paper, the technique is

easily adaptable to reflection devices by the addition of an optical switch downstream of the DUT. The single-scan, accurate, and high dynamic range measurements yielded by this technique make it ideal for rapid, high-resolution characterization of passive optical components.

References and Notes

1. The linear transfer function is the two-by-two matrix, $\vec{H}(\omega)$, that relates the input and output electric field vectors of an optical system in the spectral domain according to $\vec{E}_{out}(\omega) = \vec{H}(\omega)\vec{E}_{in}(\omega)$. We use the transfer function nomenclature because, whereas the Jones matrix describes only the transfer of the polarization state, the transfer function also contains the average loss (insertion loss) and phase (chromatic dispersion).
2. D. Sandel, N. Reinhold, G. Heise, and B. Borchert, "Optical network analysis and longitudinal structure characterization of fiber Bragg grating," *J. Lightwave Technol.* **16**, 2435–2442 (1998).
3. G. D. VanWiggeren, A. R. Motamedi, and D. M. Baney, "Single-scan interferometric component analyzer," *IEEE Photon Technol Lett.* **15**, 263–265 (2003).
4. U. Glombitza and E. Brinkmeyer, "Coherent frequency domain reflectometry for characterization of single-mode integrated optical waveguides," *J. Lightwave Technol.* **11**, 1377–1384 (1993).
5. M. Froggatt, T. Erdogan, J. Moore, and S. Shenk, "Optical frequency domain characterization (OFDC) of dispersion in optical fiber Bragg gratings," in *Bragg Gratings, Photosensitivity and Poling in Glass Waveguides*, OSA Technical Digest Series (Optical Society of America, Washington, D.C., 1999), paper FF2.
6. R. Passy, N. Gisin, J. P. von der Weide, and H. H. Gilden, "Experimental and theoretical investigations of coherent OFDR with semiconductor laser sources," *J. Lightwave Technol.* **12**, 1622–1630 (1994).
7. Misalignment of either polarization controller such that the proper orthogonality conditions are not met can lead to errors in the measurement. However, for these experiments the polarization alignment was maintained such that any errors due to misalignment were much less than other sources of error in the measurement.
8. B. L. Heffner, "Automated measurement of polarization mode dispersion and using Jones matrix eigenanalysis," *IEEE Photon. Technol. Lett.* **4**, 1066–1069 (1992).
9. A. Motamedi, B. Szafraniec, P. Robrish, and D. M. Baney, "Group delay reference artifact based on molecular gas absorption," in *Optical Fiber Communication*, OSA Technical Digest Series (Optical Society of America, Washington, D.C., 2001), paper ThC8-1.
10. B. L. Heffner, "Deterministic, analytically complete measurement of polarization dependent transmission through optical devices," *IEEE Photon. Technol. Lett.* **4**, 451–454 (1992).